

SCUBE3 regulation of early lung cancer angiogenesis and metastatic progression

Cheng-Hung Chou · Yi-Fang Cheng ·
Tiing Yee Siow · Amit Kumar · Konan Peck ·
Chen Chang

Received: 3 July 2012 / Accepted: 1 February 2013 / Published online: 19 February 2013
© Springer Science+Business Media Dordrecht 2013

Abstract Signal peptide-CUB-EGF-like domain-containing protein 3 (SCUBE3) is strongly expressed in extremely invasive lung carcinoma. We showed in our previous study that SCUBE3 triggers the transforming growth factor- β pathway and subsequently promotes tumor angiogenesis and the epithelial–mesenchymal transition (EMT). However, the role of SCUBE3 in early tumor expansion hasn't been fully demonstrated in vivo. The present study used dynamic contrast-enhanced magnetic resonance imaging (DCE-MRI) to temporally assess tumor angiogenesis in SCUBE3-knockdown and control non-small-cell lung carcinoma (NSCLC) cancer cells in the early tumor stage (weeks 1–3). We further evaluated the metastatic potential of the SCUBE3-knockdown and control tumor cells using a circulating tumor cell (CTC) assay. The differences in gene expression profile between these cell lines were determined using microarray analysis. The results show that SCUBE3 knockdown was associated with lower vascular permeability in the tumor and effectively inhibited the metastatic potential of NSCLC, as evidenced by the decreased CTCs in the mice bearing SCUBE3-knockdown tumors. Microarray analysis revealed that several genes involved in angiogenesis and EMT were down-regulated in SCUBE3-knockdown tumors, including matrix metalloproteinases (MMPs) 2, 9, and 14, (*MMP-2*,

MMP-9, and *MMP-14*, respectively), fibronectin (*FN-1*), lysyl oxidase (*LOX*), hairy/enhancer-of-split related with YRPW motif protein 1 (*HEY1*), early growth response protein 1 (*EGR1*), and interleukin 8 (*IL-8*). Together these data suggest that SCUBE3 is a potential target for pharmacological intervention. The findings of the present study also show that differences in vascular permeability precede the CTCs detection, indicating that DCE-MRI may be a sensitive biomarker for assessing tumor invasiveness.

Keywords SCUBE3 · NSCLC · Angiogenesis · EMT · DCE-MRI

Abbreviations

| | |
|---------|---|
| AHNAK | Neuroblast differentiation-associated protein AHNAK |
| ANGPTL4 | Angiopoietin-related protein 4 |
| CTC | Circulating tumor cell |
| CXCL10 | C-X-C motif ligand 10 |
| DCE-MRI | Dynamic contrast-enhanced magnetic resonance imaging |
| ECM | Extracellular matrix |
| EGR1 | Early growth response protein 1 |
| EMT | Epithelial-mesenchymal transition |
| FN | Fibronectin |
| FOV | Field of view |
| GCOS | GeneChip Operating System |
| Gd-DTPA | Gadolinium-diethylenetriamine pentaacetic acid |
| H&E | Hematoxylin and eosin |
| HEY1 | Hairy/enhancer-of-split related with YRPW motif protein 1 |
| IL-8 | Interleukin 8 |
| LOX | Lysyl oxidase |
| MMP | Matrix metalloproteinases |

Cheng-Hung Chou and Yi-Fang Cheng contributed equally.

C.-H. Chou · Y.-F. Cheng · T. Y. Siow · A. Kumar · K. Peck ·
C. Chang (✉)
Institute of Biomedical Sciences, Academia Sinica,
Taipei, Taiwan
e-mail: bmcchen@ibms.sinica.edu.tw

T. Y. Siow
Far Eastern Memorial Hospital, Pan-Chiao, Taipei, Taiwan

| | |
|--------------|---|
| NEX | Number of excitation |
| NOD-SCID | Nonobese diabetic-severe combined immunodeficiency |
| NSCLC | Non-small-cell lung carcinoma |
| PAI | Plasminogen activator inhibitor |
| PBS | Phosphate-buffered saline |
| SCUBE3 | Signal peptide-CUB-EGF-like domain-containing protein 3 |
| Slth | Slice thickness |
| SMAD | Mothers against decapentaplegic homolog |
| T2WI | T ₂ -weighted images |
| TE | Echo time |
| TGF- β | Transforming growth factor- β |
| TR | Repetition time |
| VEGF | Vascular endothelial growth factor |

Introduction

It has been shown that signal peptide-CUB-EGF-like domain-containing protein 3 (SCUBE3) is strongly expressed in extremely invasive lung carcinomas and is correlated with the invasiveness of neoplastic cells [1]. As demonstrated in an in vitro study [1], SCUBE3 activates transforming growth factor- β (TGF- β) type II receptors through the C-terminal CUB domain, and triggers the canonical signaling pathway involving mothers against decapentaplegic homolog (SMAD)2/3 phosphorylation. The increase in SMAD2/3 transcriptional activity subsequently up-regulates downstream target genes, including *TGF- β 1*, *Snail*, and *Slug*, and the genes encoding plasminogen activator inhibitor (PAI)-1 (*PAI-1*), matrix metalloproteinases (MMPs) 2 and 9 (*MMP-2* and *MMP-9*, respectively), and vascular endothelial growth factor (VEGF).

The zinc-finger transcriptional factors Snail and Slug are the key effectors of the epithelial-mesenchymal transition (EMT) process, by virtue of their repressive effect on E-cadherin expression [2–4]. Loss of E-cadherin from the adherens junctions renders the tumor cell motile, which is a prerequisite for transforming into an invasive phenotype. While the EMT process endows tumor cells with migratory properties, the metalloproteinases up-regulated by SCUBE3, MMP-2, and MMP-9 further enhance the invasiveness of tumor cells by degrading the extracellular matrix (ECM) and allowing the passage of tumor cells through the connective tissue. Nonetheless, the gene encoding VEGF, the most important and recognized tumor angiogenic factor, is also up-regulated by the SCUBE3-TGF- β -receptor signaling pathway. The formation of new blood vessels by angiogenesis provides the principal conduit for tumor cell metastasis, in addition to supplying the cancer cells with the vital nutrients and oxygen necessary for continuing tumor growth.

These downstream molecules up-regulated by SCUBE3 act in a coordinated autocrine or paracrine manner to orchestrate a neoplastic microenvironment that favors tumor progression, invasion, and metastasis.

In our previous in vivo study [1], the tumorigenesis effect of SCUBE3 was reflected in the macroscopic reduction in tumor size after SCUBE3 knockdown. The subcutaneously transplanted tumor in mice was significantly smaller in SCUBE3-knockdown tumors than in controls after 4 weeks. However, the role of SCUBE3 in the preceding events in the tumor microenvironment remains obscure. Therefore, the aim of the present study was to further characterize the function of SCUBE3 in early tumor expansion during the first 3 weeks.

Angiogenesis is undoubtedly an integral part of solid tumor development [5]. It is characterized by the formation of disorganized and structurally defective new vessels with high permeability and fragility. This property is exploited by dynamic contrast-enhanced magnetic resonance imaging (DCE-MRI) for angiogenesis imaging. Technically, DCE-MRI involves the rapid acquisition of a series of T₁-weighted images following the injection of an intravenous bolus of contrast agent [usually gadolinium-diethylenetriamine pentaacetic acid (Gd-DTPA)]. Vessels with different permeabilities produce different enhancements with the contrast agent. Through pharmacokinetic modeling of contrast agents, vascular parameters [e.g., vascular permeability (K^{trans})] can be derived to reflect the functional status of tumor microcirculation. It was previously reported that the value of K^{trans} was strongly correlated with microvascular density on immunohistochemistry staining [6], and with the level of VEGF expression [7]. It was also shown to be correlated with the prognosis of many human cancers [8–10]. In the present work, we attempted to utilize this imaging modality as a means of monitoring the temporal changes in the vasculature of SCUBE3-knockdown non-small-cell lung carcinoma (NSCLC) tumors. The metastatic potential of the cancer was assessed by detecting and enumerating circulating tumor cells (CTCs). The differences in the gene expression profiles of SCUBE3-knockdown and control tumors were analyzed with the aid of microarray analysis.

We found that tumor angiogenesis was significantly suppressed in the SCUBE3-knockdown tumors, as evidenced by K^{trans} being lower than in the control condition. However, the tumor size did not differ between the knockdown and control conditions at week 3, which is consistent with previous report [1]. Our data also suggest that SCUBE3 knockdown can effectively inhibit the metastatic potential of NSCLC, as evidenced by the decreased CTCs in SCUBE3-knockdown tumors. Furthermore, gene expression profiling revealed that several genes involved in angiogenesis and EMT were down-regulated in SCUBE3-knockdown tumors, including *MMP-2*, *MMP-9*, and

MMP-14, as well as those encoding fibronectin (FN), lysyl oxidase, hairy/enhancer-of-split related with YRPW motif protein 1, early growth response protein 1, and interleukin 8 (*FN-1*, *LOX*, *HEY1*, *EGR1*, and *IL-8*, respectively). These data suggest that SCUBE3 is a logical target for pharmacological intervention in the treatment of NSCLC. Moreover, we found that differences in K^{trans} preceded the detection of CTCs, indicating that DCE-MRI may be a sensitive biomarker for assessing tumor invasiveness.

Materials and methods

Cell culture and animal model

Human lung adenocarcinoma SCUBE3-knockdown cells [CL1-5(shSCUBE3)] and control cells [CL1-5(shLacZ)] were kind gifts from Dr. Pan-Chyr Yang (Department of Internal Medicine, National Taiwan University Hospital, Taipei, Taiwan) [1]. The cells were cultured in RPMI 1640 medium supplemented with 25 mM 4-(2-hydroxyethyl)-1-piperazineethanesulfonic acid, 0.75 $\mu\text{g}/\text{mL}$ puromycin, and 10 % fetal bovine serum. For tumor implantation, 5×10^6 CL1-5(shLacZ) or CL1-5(shSCUBE3) cells were injected subcutaneously into 8-week-old male non-obese diabetic-severe combined immunodeficiency (NOD-SCID) mice. Animal experiments were performed using protocols approved by the Academia Sinica Institutional Animal Care and Utilization Committee.

MRI

All magnetic resonance images were acquired at weeks 1, 2, and 3 on a horizontal 7.0-T PharmaScan 70/16 spectrometer with a 38-mm volume coil, which was used as both a transmitter and a receiver. Each mouse ($n = 26$) was first anesthetized by inhalation of 5 % isoflurane in air at a flow rate of 5 L/min, and then placed onto a mouse body holder in a prone position. A catheter with a needle was set up to enable the injection of contrast medium into the orbital veins. During the scanning, anesthesia was maintained via inhalation with 1–2 % isoflurane in air at 2 L/min; warmed air was pumped into the magnet bore to maintain the body temperature.

Tumor volume measurement

T_2 -weighted images (T2WIs) were acquired for tumor volume measurement with a fast spin-echo sequence with a repetition time (TR) of 5000 ms, an effective echo time (TE) of 50 ms, an echo train length of 8 echoes, a field of view (FOV) of 4×4 cm, an acquisition matrix size of 256×128 (zero-padded to 256×256), a slice thickness (Slth) of 0.5 mm, and number of excitation (NEX) of 2. The number of slices was chosen to cover the entire tumor.

The tumor region in each slice was defined and selected using Avizo software (TGS, San Diego, CA, USA). The tumor volume was calculated from the selected area of each slice.

DCE-MRI

The permeability of tumor vessels was assessed by K^{trans} maps from DCE-MRI. DCE-MRI was performed as dynamic T_1 -weighted images of the gradient echo sequence with a flip angle of 30° , TR of 140 ms, TE of 3 ms, FOV of 3×3 cm, Slth of 1.5 mm, NEX of 1, and an acquisition matrix size of 128×128 (zero filled to 256×256). A dynamic series of 80 axial images was obtained; Gd-DTPA [Magnevist (MW: 938 Da), Schering, Berlin, Germany] was injected at 8th image acquisition at a dose of 0.2 mmol/kg.

Image analysis

The Gd-DTPA-enhanced kinetic signals were analyzed based on the compartment model of Tofts [11, 12]. The transfer rate of the contrast agent was described by $dCt(t)/dt = K^{\text{trans}} \times (C_p - Ct/v_e)$, where Ct is the concentration of contrast agent in the tissue extravascular and extracellular spaces, K^{trans} is the vascular permeability, C_p is the concentration of contrast agent in the plasma space, and v_e is the leakage space per unit volume of measured tissue. Optimal values of the pharmacokinetic parameters, K^{trans} and v_e , were calculated by applying nonlinear regression analysis to fit the dynamic curve of the tissue signal on each pixel. The processing program for the fitting was written using MATLAB software (MathWorks, Natick, MA, USA). The K^{trans} map of the tumor was segmented and superimposed on T2WIs, while the segmented K^{trans} map is presented as a color map using Avizo software (TGS, San Diego, CA, USA).

Immunohistochemistry staining

The mice were sacrificed under chloral hydrate anesthesia at week 3. Tumor specimens were harvested, fixed in 4 % paraformaldehyde overnight, and then dehydrated with a series of alcohol solutions in an automatic machine. The specimens were subsequently embedded in paraffin blocks and sectioned at 5 μm using a rotary microtome (Sakura Accu-Cut SRM, Sakura Finetek, Torrance, CA, USA). The sections were stained with hematoxylin and eosin (H&E) to enable examination of the tumor morphology.

For immunohistochemistry staining, slices were incubated with 3 % H_2O_2 in phosphate-buffered saline (PBS) to block the endogenous peroxidase. The antigen target was heated for 30 min in antigen target retrieval solution for

antigen retrieval. The slices were subsequently incubated with blocking solution (3 % donkey serum, 2 % bovine serum albumin, and 0.1 % Triton X-100 in 1× PBS) for 1 h. The primary antibody, polyclonal goat antimouse CD31 (SC-1506, Santa Cruz Biotechnology, Santa Cruz, CA, USA), was diluted at 1:100 and applied to the slices, which were then incubated at room temperature overnight. After washing, the slices were incubated with biotinylated donkey antigoat secondary antibody (705-066-147, Jackson Immuno Research Laboratories, West Grove, PA, USA) at a dilution of 1:1,000 for 1 h. The slices were washed and then incubated in avidin–biotin peroxidase complex (PK6100, Vectastain Elite ABC standard kit, Vector Labs, Burlingame, CA, USA) for 1 h. The color was developed using 3,3'-diaminobenzidine (D5637, Sigma-Aldrich, St. Louis, MO, USA) to give a brown color. Hematoxylin (008011, Invitrogen, Carlsbad, CA, USA) was used as a counterstain (blue). Vessel density and vessel size were calculated by measuring the number of vessels and the fiber breadth using Metamorph software (Universal Imaging, West Chester, PA, USA).

Analysis of gene profiling by Affymetrix GeneChip

NOD-SCID mice were implanted with 5×10^6 CL1-5(shLacZ) or CL1-5(shSCUBE3) cells. Three tumor samples from each experimental group were harvested at weeks 2 and 3. Three tumor samples from each experimental group were harvested at weeks 2 and 3 for total RNA isolation using the MaestroZol RNA Extraction Reagent (Maestrogen, Las Vegas, NV, USA) according to the manufacturer's protocols. Samples of the same group collected at the same time point were pooled together for microarray analysis. Human genome U133 Plus 2.0 GeneChip oligonucleotide arrays (Affymetrix, Santa Clara, CA, USA) were used in this study. The processing of the Affymetrix GeneChip, including cDNA and cRNA synthesis, labeling, hybridization, scanning, and data analysis using the GeneChip Operating System (GCOS), were performed at the National Research Program for Genomic Medicine Microarray and Gene Expression Analysis Core Facility (Academia Sinica, Taipei, Taiwan) according to the manufacturer's instructions (Affymetrix). All expression levels of the genes were determined in the GCOS absolute analysis using the global scaling option. The GCOS comparison analysis algorithm was used to compare the gene expression levels between two samples. Genes with differential expression levels between weeks 2 and 3 were selected by passing the criteria of showing a Change Call "I" or "D" and signal \log_2 ratio $\geq +1$ or ≤ -1 in both comparisons of CL1-5(shLacZ)_{3w/2w} and CL1-5(shSCUBE3)_{3w/2w}. The heat maps of differentially expressed genes were derived from Genesis software version 1.7.5

[13] based on *k*-means clustering. The functional annotations and pathway analyses of differentially expressed genes were performed using MetaCore software (GeneGo, Encinitas, CA, USA).

In vivo assay of human tumor cell invasiveness

The invasiveness of CL1-5(shLacZ) and CL1-5(shSCUBE3) cells was measured by detecting the CTCs in the mouse circulatory system. Genomic DNA of peripheral blood was extracted using a QIAamp DNA Blood Mini Kit (Qiagen, Hilden, Germany) according to the manufacturer's protocols. The amount of CTCs in the mouse circulatory system was determined by measuring the human Alu sequence in genomic DNA from mouse peripheral blood by real-time quantitative polymerase chain reaction [14]. The tumor volume was measured with calipers using the formula $V = ab^2/2$, where V is the tumor volume, a is the length and b is the width of the tumor [15].

Statistical analysis

Data are expressed as mean and SE values. The data were analyzed by Student's *t* test, and the level of statistical significance was set at $p < 0.05$.

Results

Tumor size measured on T2WIs

The volumes of CL1-5(shLacZ) and CL1-5(shSCUBE3) tumors were measured in T2WIs (Fig. 1). At week 1 the CL1-5(shSCUBE3) tumors were significantly larger than the CL1-5(shLacZ) tumors ($p = 0.024$). The volumes of both CL1-5(shSCUBE3) and CL1-5(shLacZ) tumors increased with time, and did not differ significantly between them at weeks 2 ($p = 0.103$) and 3 ($p = 0.698$).

Permeability (K^{trans} map) of the tumor vessels

The region of the tumor core was defined as 50 % of the distance from the central point of the tumor to its outside boundary, while the region of the tumor rim was determined by subtracting the area of the tumor core from that of the total tumor area (as illustrated in Fig. 2a) [16]. The K^{trans} values of CL1-5(shLacZ) and CL1-5(shSCUBE3) tumors are presented as a color map, from blue (low) to red (high) on a T2WI reference at weeks 1, 2, and 3 (Fig. 2b). In both the CL1-5(shLacZ) and CL1-5(shSCUBE3) tumors, vessels with increased permeability were observed at the tumor periphery at week 1. The K^{trans} values did not differ significantly between CL1-5(shLacZ) and CL1-5(shSCUBE3) tumors at

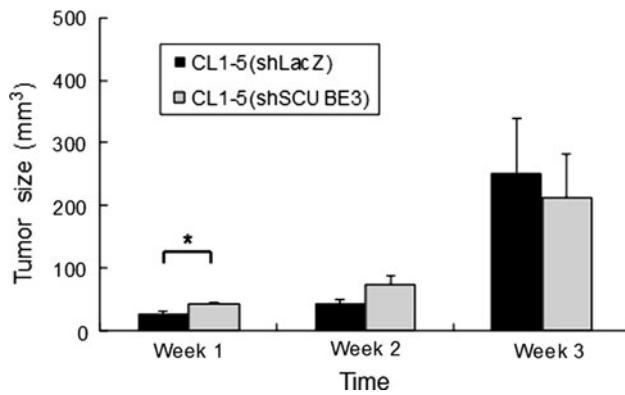


Fig. 1 Tumor growth curve. The tumor volume was measured on T2WIs. At week 1 the CL1-5(shSCUBE3) tumors were significantly larger than the CL1-5(shLacZ) tumors. There was no significant difference at weeks 2 and 3 between CL1-5(shLacZ) and CL1-5(shSCUBE3) tumors. * $p \leq 0.05$

either the tumor rim ($p = 0.130$) or tumor core ($p = 0.946$) at this time point. At week 2 K^{trans} had increased at both the rim and core regions of CL1-5(shLacZ) and CL1-5(shSCUBE3) tumors, but there was still no significant difference between CL1-5(shLacZ) and CL1-5(shSCUBE3) tumors at the tumor rim ($p = 0.956$) or the tumor core ($p = 0.545$). The K^{trans} values of CL1-5(shLacZ) tumors remained stagnant at week 3 in both the tumor core and rim, where those of CL1-5(shSCUBE3) tumors were decreased throughout the tumor. At week 3 the K^{trans} values were significantly lower for the CL1-5(shSCUBE3) tumors than for CL1-5(shLacZ) tumors in both the core ($p = 0.029$) and the rim ($p = 0.043$).

Tumor morphology and quantification of vessel density and size

CL1-5(shLacZ) and CL1-5(shSCUBE3) tumors were harvested and stained with H&E at week 3 (Fig. 3a). The CL1-5(shSCUBE3) tumors exhibited necrosis at the central core. The selected areas of the tumor core (green box) and tumor rim (blue box) are shown at a higher magnification. The regions numbered 1–5 are shown at high magnification in the insets. The cell nucleus had a solid morphology in region 1 of CL1-5(shLacZ) tumors, but cells exhibited apoptotic morphology in region 5 of CL1-5(shSCUBE3) tumors. Mitotic features were observed in the cell nuclei in regions 2 and 3. Red blood cells were stained in region 4.

Figure 3b shows vessels stained by CD31 antibodies immunohistochemically (brown). The selected areas of the tumor core (green box) and tumor rim (blue box) are shown at a higher magnification. Vessel density and size were quantified using Metamorph software (Fig. 3c, d). The vessel density was significantly higher for CL1-5(shLacZ) tumors than for CL1-5(shSCUBE3) tumors ($p = 0.0002$) at

the core. The vessel density did not differ significantly ($p = 0.214$) between CL1-5(shLacZ) and CL1-5(shSCUBE3) tumors at the rim. The vessel size of CL1-5(shSCUBE3) tumors in the core was significantly larger than that of CL1-5(shLacZ) ($p = 0.00005$). Both CL1-5(shLacZ) and CL1-5(shSCUBE3) tumors had similar vessel size at the rim ($p = 0.068$).

Gene expression profiling by microarray analysis

The gene expression profiles of four groups of tumor tissues, comprising 2-week-old and 3-week-old CL1-5(shLacZ) and CL1-5(shSCUBE3) tumors, were analyzed using Affymetrix GeneChip technology. To find out the genes which correlated with the vascular phenotype change between weeks 2 and 3, genes whose expression changed by more than twofold between weeks 2 and 3 in either kind of tumor cells were selected. As shown in Fig. 4a, the genes could be categorized into three clusters according to their specific expression patterns. The genes in the top cluster had expression levels that were lower in the control tumor than in the SCUBE3-knockdown tumor at week 3. The middle cluster comprises genes whose expression levels were higher in the control tumor than in the SCUBE3-knockdown tumor at week 3. The expression levels of the genes in the bottom cluster were similar between the control and SCUBE3-knockdown tumors at week 3.

The differentially expressed genes were analyzed using MetaCore software to identify the possible involved pathways. Among the mapped pathways, genes involved in the processes of angiogenesis and EMT were selected for further analysis. Figure 4b shows the heat map of these genes, with their public IDs, gene symbols, and gene titles listed from left to right beside them. The expression levels of these genes at week 3 were compared between CL1-5(shLacZ) and CL1-5(shSCUBE3) tumors and plotted as the relative \log_2 signal ratio. Figure 4c shows that with SCUBE3 knockdown, genes that promote angiogenesis and EMT, including *FNI*, *MMP2*, *LOX*, *HEY1*, *MMP14*, *IL-8*, *EGR1*, and the gene encoding the neuroblast differentiation-associated protein AHNAK (*AHNAK*) were down-regulated; in contrast, genes capable of inhibiting angiogenesis and EMT were up-regulated [e.g., those encoding angiopoietin-related protein 4 (*ANGPTL4*) and chemokine (C–X–C motif) ligand 10 (*CXCL10*)]. Figure 4d shows the changes in gene expression levels in CL1-5(shLacZ) and CL1-5(shSCUBE3) tumors. The expressions of *HEY1*, *MMP14*, *MMP2*, and *AHNAK* increased more between weeks 2 and 3 in CL1-5(shLacZ) tumors than in CL1-5(shSCUBE3) tumors. The expression of *ANGPTL4* increased moderately between weeks 2 and 3 in CL1-5(shLacZ) tumors, but increased even more significantly in

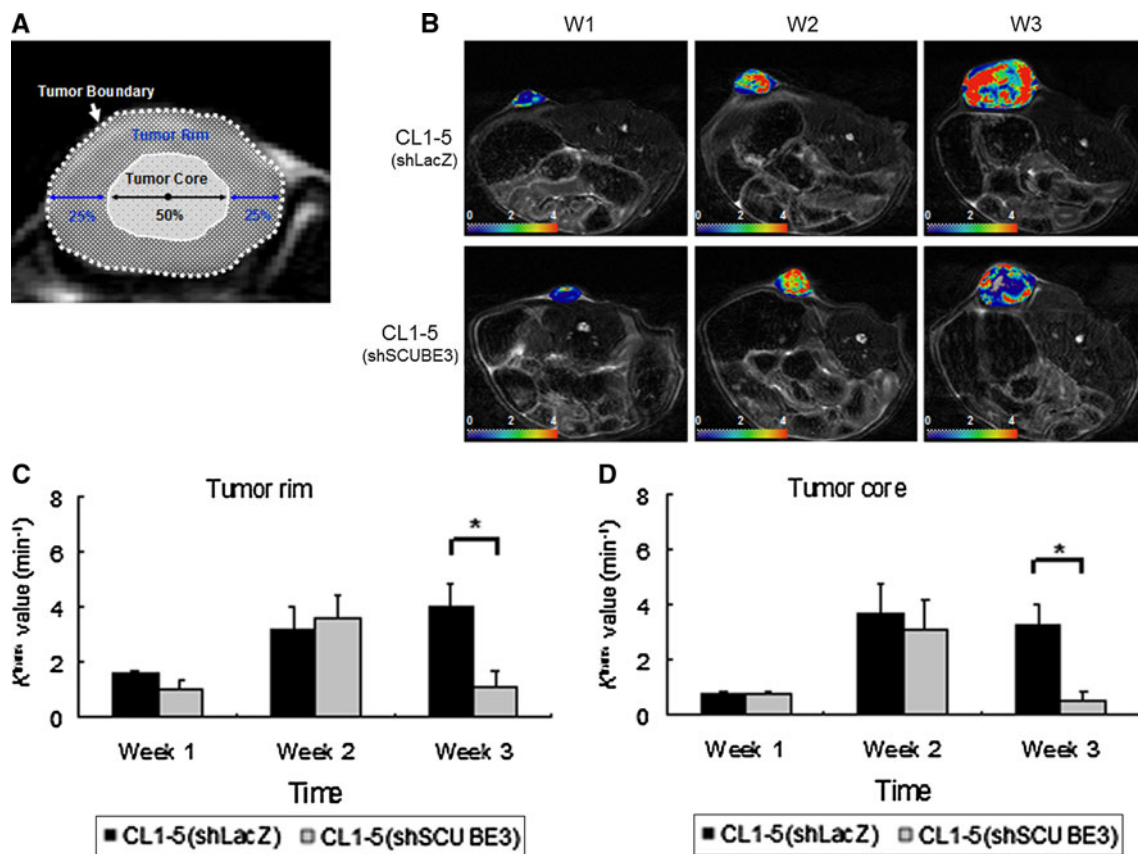


Fig. 2 Vascular permeability, as measured using K^{trans} maps. **a** The region of the tumor core was defined as 50 % of the distance from the central point of the tumor to its outside boundary, while the region of the tumor rim was determined by subtracting the area of the tumor core from that of the total tumor area. **b** Segmented K^{trans} maps of

CL1-5(shLacZ) and CL1-5(shSCUBE3) shown on T2WIs of axial views from weeks 1 (W1), 2 (W2), and 3 (W3). The false colors show K^{trans} values from 0 to 4/min. K^{trans} was calculated at the tumor rim **c** and the tumor core **d**. Data are mean and SE values. * $p \leq 0.05$

CL1-5(shSCUBE3) tumors. The expressions of *CXCL10* and the gene encoding *SMAD7* (*SMAD7*), which decreased between weeks 2 and 3 in CL1-5(shLacZ) tumors, were increased in CL1-5(shSCUBE3) tumors between the same time points.

In vivo intravasation analysis by CTC detection

No CTCs were detected during the first 3 weeks. The relative number of CTCs was normalized to the tumor size at weeks 4 and 5 after implantation (Fig. 5). At week 4 there was no significant difference in the number of CTCs between mice bearing CL1-5(shLacZ) and CL1-5(shSCUBE3) tumors ($p = 0.607$). However, the number of CTCs was significantly higher at week 5 in mice bearing CL1-5(shLacZ) tumor cells than in mice bearing CL1-5(shSCUBE3) tumor cells ($p = 0.048$). CTCs were significantly decreased at week 5 compared to week 4 in the plasma of mice bearing a CL1-5(shSCUBE3) tumor ($p = 0.0236$). CTCs in the mice with CL1-5(shLacZ) did not differ significantly ($p = 0.097$) between weeks 4 and 5.

These data show that the number of metastatic cells in circulation was decreased with SCUBE3 knockdown.

Discussion

Tumor angiogenesis and growth are regulated by SCUBE3

CL1-5(shSCUBE3) tumors were significant larger than CL1-5(shLacZ) tumors at week 1, but the tumor size did not differ significantly between the two groups at weeks 2 and 3. This observation may be due to the contextual role of TGF- β in tumor development [17]. In the early stages of tumorigenesis, TGF- β signaling exerts a suppressive effect on tumor growth by inducing cell-cycle arrest and apoptosis. In contrast, in the later stages this signaling pathway promotes tumor cell invasion and metastatic potential through the EMT process. Although our previous study [1] showed that the tumor sizes between CL1-5(shLacZ) and CL1-5(shSCUBE3) did not differ significantly until week

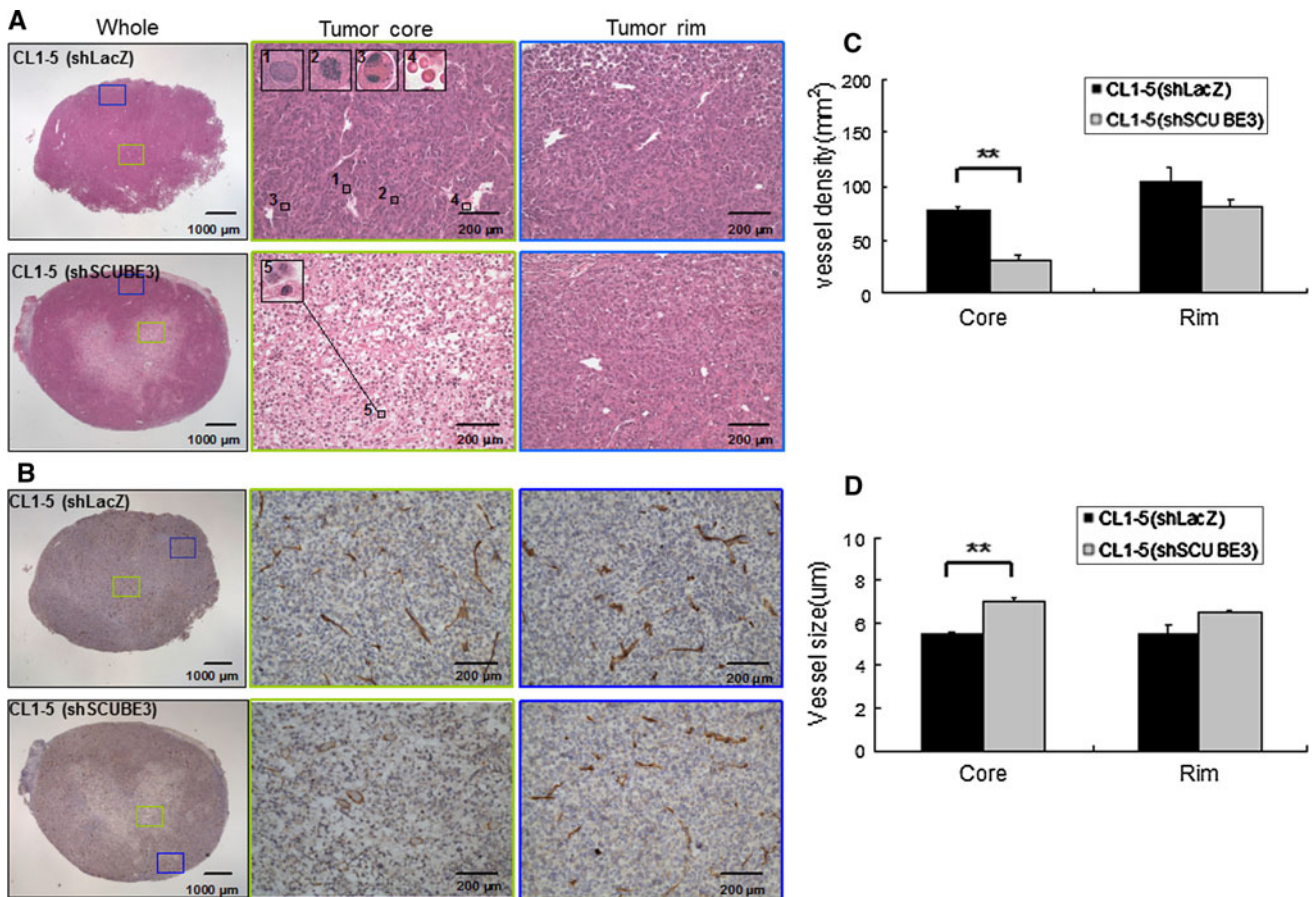


Fig. 3 Tumor morphology and quantification of vessel density and size. **a** CL1-5(shLacZ) and CL1-5(shSCUBE3) tumors were stained with H&E at week 3. The CL1-5(shSCUBE3) tumors exhibited necrosis at the central core. The regions numbered 1–5 are shown at high magnification in the insets. The cell nucleus had a solid morphology in region 1 of CL1-5(shLacZ) tumors, but cells exhibited apoptotic morphology in region 5 of CL1-5(shSCUBE3) tumors. Mitotic features were observed in the cell nuclei in regions 2 and 3.

Red blood cells were stained in region 4. **b** Vessels were stained brown by CD31 antibodies immunohistochemically. The selected areas of the *tumor core* (green box) and *tumor rim* (blue box) are shown at a higher magnification. In CL1-5(shLacZ) and CL1-5(shSCUBE3) tumors, vessel density (**c**) and vessel size (**d**) were calculated by counting the number of vessels and measuring their size using Metamorph software. Data are mean and SE values. ****** $p \leq 0.01$

4. However, present study showed that there was a significant difference between CL1-5(shLacZ) and CL1-5(shSCUBE3) tumors at week 1. This difference in observations is probably due to different methods of measurement being applied. In present study tumor sizes were calculated from the summation of the tumor occupying voxels as shown in T_2 -weighted images. Measurement was done with calipers using the formula $V = ab^2/2$ (as mentioned earlier) in previous study.

Examination of tumor histology at week 3 revealed that SCUBE3 knockdown caused both tumor necrosis and inhibited angiogenesis in the core region. One possible explanation for this is that SCUBE3 knockdown inhibits VEGF expression, which causes deprivation of oxygen and nutrients for tumor cells due to inadequate neovascularization. However, it could also be that tumor necrosis

induced by SCUBE3 knockdown decreases the amount of cytokine secreted to stimulate angiogenesis.

Together the MRI and histological results suggest that SCUBE3 knockdown can reduce the viable-tumor burden. Since the sizes of SCUBE3-knockdown and control tumors did not differ significantly at week 3, while the histological examination revealed marked tumor necrosis in SCUBE3-knockdown tumors; it is thus apparent that the viable-tumor volume was smaller in the SCUBE3-knockdown tumor.

SCUBE3 regulates genes involved in angiogenesis and tumor growth

Microarray studies have captured a differential gene expression profile between SCUBE3-knockdown and control tumors. As shown in Fig. 4a, several genes that are

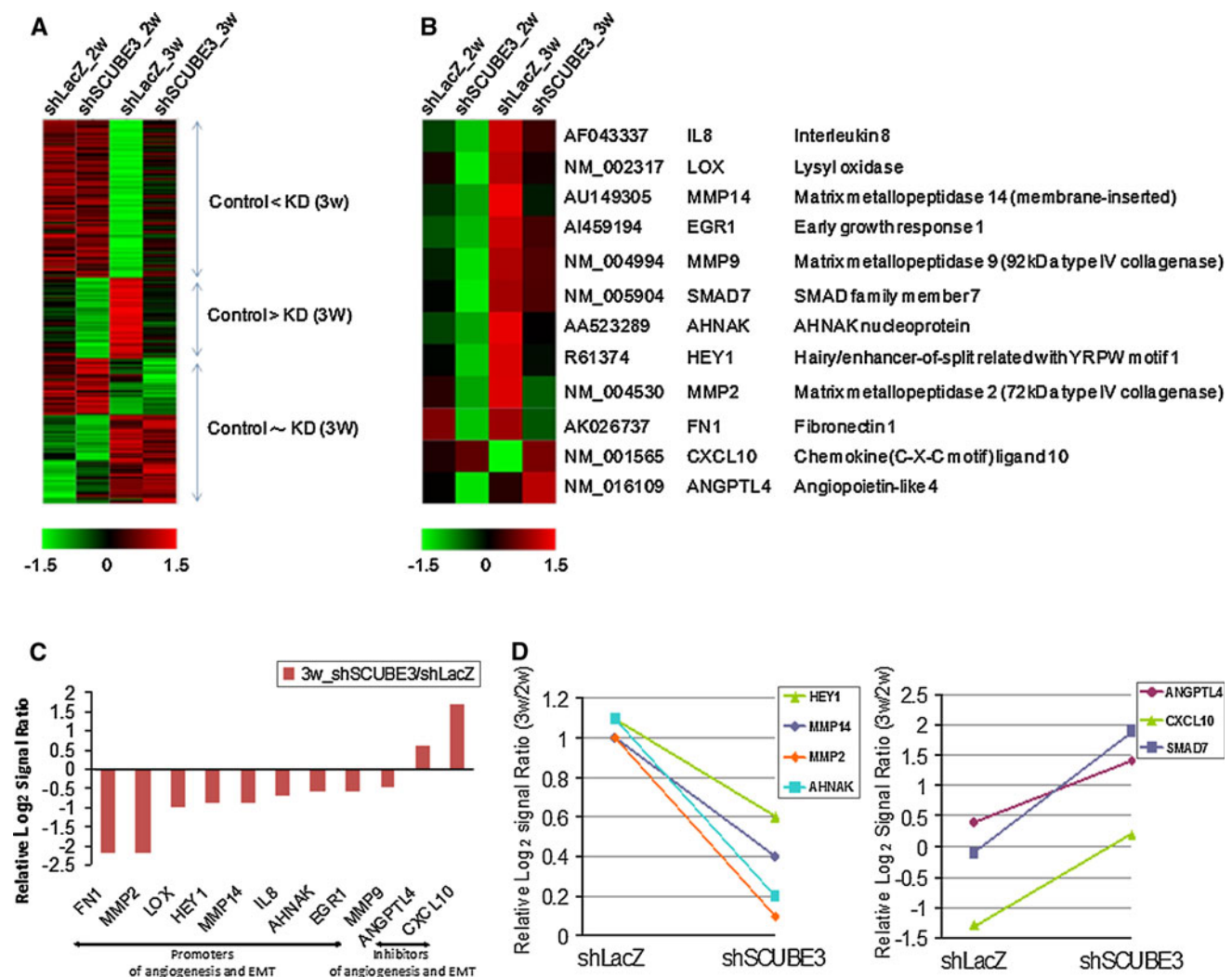


Fig. 4 Effect of SCUBE3 knockdown on gene expression profiling. **a** Heat map of the genes for which expression changed by more than twofold between weeks 2 and 3 in either kind of tumor cell. Genes in the *top cluster* are those for which the expression was lower in the control tumor than in SCUBE3-knockdown tumor at week 3. The expression of those in the *middle cluster* was higher in the control tumors than in the SCUBE3-knockdown tumors at week 3. The expression of those in the *bottom cluster* was similar in the control

involved in angiogenesis and tumor progression were regulated by SCUBE3. For example, the genes encoding MMPs, which are known to play pivotal roles in promoting tumor invasion, metastasis, and angiogenesis, were down-regulated after SCUBE3 knockdown. MMPs promote tumor angiogenesis by degrading type IV collagen of the vascular basal lamina to facilitate endothelial cells migration and capillary sprouting. In particular, MMP-2 could directly bind to $\alpha_v\beta_3$ receptors to initiate integrin signaling to promote endothelial cell survival and proliferation [18–20]. MMPs can also potentiate tumor angiogenesis by cleaving ECM-bound proangiogenic factors (e.g., basic fibroblast growth factor and VEGF) [21–23]. Moreover,

and SCUBE3-knockdown tumors at week 3. **b** Heat map of genes involved in angiogenesis and EMT (MetaCore). The public IDs, gene symbols, and gene titles are listed from *left to right beside* the heat map. **c** Comparison of gene expression levels between CL1-5(shLacZ) and CL1-5(shSCUBE3) tumors at week 3, plotted as relative log₂ signal ratio of CL1-5(shSCUBE3) to CL1-5(shLacZ). **d** Plot of relative log₂ signal ratio [week 3/week 2 (3w/2w)] to show the temporal changes in gene expression levels of both tumors

MMPs act on the latent TGF- β complex through proteolytic activation, hence activating the aforementioned TGF- β pathway to increase production of VEGF. The up-regulation of *MMP-2* and *MMP-9* has been reported to be a poor prognostic factor in NSCLC [24]. In addition, genes that are related to the transcription of MMPs were also down-regulated with SCUBE3 knockdown. The expression of *EGR1*, which encodes a transcription factor that is essential in the induction of *MMP-9* transcription by tumor necrosis factor- α [25], was decreased after SCUBE3 knockdown.

Our previous work using Western blotting has revealed that, VEGF is upregulated by SCUBE3-TGF- β signaling

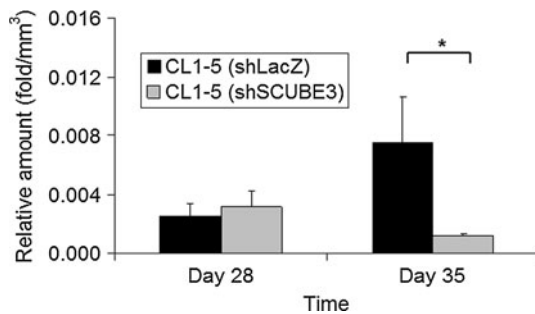


Fig. 5 Quantitative measurement of CTCs. Circulating CL1-5 tumor cells were quantitatively measured using the real-time quantitative polymerase chain reaction for the human Alu sequence ($n \geq 5$). The relative number of CTCs was normalized to the tumor size. Data are mean and SE values. * $p \leq 0.05$

pathway. In present study, data from microarray supports similar notion, with increased gene expression of VEGF-A in CL1-5(shLacZ) compared to CL1-5(shSCUBE3) at week 3 (signal \log_2 ratio = 0.6). However, when considering signal ratio of CL1-5(shSCUBE3_3w/2w (signal \log_2 ratio = 0.7) and CL1-5(shLacZ)_3w/2w (signal \log_2 ratio = 0.3), both did not pass our selection criteria for analysis (signal \log_2 ratio > 1).

Our previous study had shown that SCUBE3 CUB domain is sufficient to bind T β R-II and induce Smad2/3 phosphorylation [1]. In present study, we examined the possible role of the endogenous ligand of T β R-II, TGF- β 1, in SCUBE3-TGF- β -receptor signaling pathway. We found that microarray data showed no differences in TGF- β 1 gene expression levels between CL1-5(shSCUBE3) and CL1-5(shLacZ) tumors at weeks 2 and 3. Taken together with our previous result that SCUBE3-induced Smad2/3 phosphorylation was not affected by TGF- β neutralizing antibody [1], it is reasonable to conclude that the activation of T β R-II by SCUBE3 is mainly through direct binding of SCUBE3 to the receptor, rather than through upregulation of endogenous TGF- β .

Microarray analysis also showed that *FN1* was down-regulated with SCUBE3 knockdown. FN is a matrix glycoprotein implicated in several types of cancer [26–28]. It was previously shown that the FN expression is increased in NSCLC [27]. FN binds to the $\alpha_v\beta_1$ receptor and is involved in multiple signaling pathways, including activation of Akt/mTOR/p70S6 K and inhibition of phosphatase and tensin homolog and liver kinase B1/5' AMP-activated protein kinase signaling [29]. It was indicated that FN contributes to a VEGF-independent angiogenesis pathway that is important for tumor growth [30]. Moreover, FN is known to be a marker of EMT, and has been shown to promote the metastatic potential of cancer cells [31, 32].

An especially notable finding was that the knockdown of SCUBE3 was associated with the down-regulation of

angiogenic chemokine and up-regulation of angiostatic chemokine. For example, IL-8 was down-regulated with SCUBE3 knockdown. IL-8 is a potent neutrophil chemo-attractant, the expression of which has been linked to increased neutrophil infiltration and neutrophil-dependent tumor angiogenesis [33]. In addition, IL-8 signaling has been shown to induce the phosphorylation of the VEGF receptor in endothelial cells in vitro [34]. Its expression is also strongly correlated with tumor angiogenesis in numerous in vivo models [35–38]. In contrast, CXCL10 represents an angiostatic chemokine [39, 40] that is up-regulated after SCUBE3 knockdown.

The lower K^{trans} values in CL1-5(shSCUBE3) tumors may be attributable to the decreased VEGF and increased ANGPTL4 levels associated with SCUBE3 knockdown. In addition to being an angiogenic factor, VEGF is also a key determinant in promoting vascular permeability [41]. In contrast, ANGPTL4 acts as an antipermeability factor that stabilizes the vessel and facilitates vascular maturation. A previous study [42] found that ANGPTL4 molecules could inhibit histamine- and VEGF-induced vessel leakiness, although it did not affect the density of blood vessels in tumor. It is postulated that *ANGPTL4* is a tumor-suppressor gene that exerts antimetastatic effects on cancer by inhibiting vascular permeability and subsequently preventing tumor cell intravasation.

SCUBE3 regulation on genes involved in metastasis

As shown in Fig. 4c, several genes that are involved in EMT, such as *HEY1*, *LOX*, and *AHNAK*, were down-regulated after SCUBE3 knockdown. *HEY1* is an established target of Notch signaling. There is emerging evidence of a link between the Notch pathway and progression of cancer, including NSCLC [43]. Sahlgren et al. [44] showed that Notch signaling adopts two mechanisms to influence EMT: (1) directly up-regulating *Snail-1* expression by the recruitment of Notch1 intracellular domain to the *Snail-1* promoter, and (2) recruiting hypoxia-induced factor α to the *LOX* promoter to increase *LOX* expression. The *LOX* gene encodes an enzyme that catalyzes the covalent cross-link of the component side chains of collagen and elastin, which is critical in ECM stabilization and maturation. However, paradoxically, *LOX* was found to be associated with cancer cell proliferation and invasiveness [45, 46]. Clinically, the *LOX* status has been reported to be a significant prognostic factor in the 5-year-survival of NSCLC [47] in patients, especially those in the early stage (stage I) [46]. Recent studies have demonstrated that *LOX* influences the EMT of cancer cells, either by directly decreasing the expression of E-cadherin or through the stabilization of *Snail-1* [44].

Actin-dependent protrusion of cell pseudopodia represents another hallmark of EMT-mediated cell invasion. As stated above, the essential protein for pseudopod protrusion, AHNAK, was down-regulated after SCUBE3 knockdown. Depletion of AHNAK protein has been shown to reverse the EMT process, causing the expression of E-cadherin, and reduce cell migration and invasiveness [48].

The knockdown of SCUBE3 resulted in the increased expression of inhibitory SMAD, namely SMAD7. A previous study showed that SCUBE3 promotes tumor angiogenesis and EMT by binding to TGF- β receptor II, and subsequently activates the canonical TGF- β -SMAD2/3 signaling pathway. SMAD7 could exert its inhibitory effect on this pathway by forming stable associations with the activated TGF- β receptor to prevent phosphorylation of SMADs [49, 50]. It was also found that SMAD7 could promote ubiquitination and degradation of the TGF- β receptors [51]. Hence, the loss of expression of SCUBE3 in tumor cells not only decreased the stimulus for the TGF- β pathway but further deactivated it via up-regulation of its inhibitory counterpart.

Metastatic tendency reduced by SCUBE3 knockdown

As discussed above, SCUBE3 involves in the regulation of several genes that are responsible for loss of cell–cell adhesion, tumor cell motility, matrix degradation, and angiogenesis, thereby modulating various dimensions of the multistep cascade for tumor metastasis. As shown in Fig. 5, knockdown of SCUBE3 effectively reduced the number of CTCs detected. In our previous work, mice that were injected intravenously with SCUBE3-knockdown cells developed significantly fewer pulmonary metastatic nodules than those injected with control cells. This implies that SCUBE3 mediates tumor cell metastasis by both facilitating tumor cell intravasation and distant colonization.

Studies have consistently demonstrated the correlation between CTCs and the prognosis and extent of disease in different types of cancer. However, our results show that the changes in K^{trans} even preceded the detection of CTCs, while high K^{trans} values were strongly correlated with the later metastatic potential of cancer cells. Presumably, the formation of leaky vasculature by angiogenesis is a prerequisite for tumor cell intravasation. Hence, the metastatic tendency of tumor cells may be indicated earlier by K^{trans} than by CTCs.

In conclusion, by different experimental approaches, the findings of the present work support the original notion that SCUBE3 plays a critical role in lung cancer invasion and metastasis, mainly via the modulation of tumor angiogenesis and EMT. Importantly, these data suggest that

inhibition of SCUBE3 is an intriguing therapeutic opportunity for controlling lung cancer metastasis at an early stage. Furthermore, these findings suggest that DCE-MRI is a sensitive modality for predicting the metastatic tendency of early cancer, rendering this tool a promising biomarker for early cancer risk stratification and thereby to guide the treatment strategy in clinical management. However, further experiments should be conducted using molecular biology-based techniques to confirm the role of SCUBE3 in the regulation of individual genes.

Acknowledgments This paper was written in memory of late Dr. Konan Peck (1958–2011) and to honor his many valuable contributions to this research project. The authors acknowledge technical support from the Functional and Micro-Magnetic Resonance Imaging Center supported by the National Research Program for Genomic Medicine, National Science Council, Taiwan, Republic of China (NSC 99-3112-B-001-020). We thank Dr. Pan-Chyr Yang (Department of Internal Medicine, National Taiwan University Hospital, Taipei, Taiwan) for providing the CL1-5 cell lines with and without SCUBE3 knockdown. We also appreciate the help of Mr. Yi-Hua Hsu with discussions on histology.

References

1. Wu YY, Peck K, Chang YL, Pan SH, Cheng YF, Lin JC, Yang RB, Hong TM, Yang PC (2011) SCUBE3 is an endogenous TGF- β receptor ligand and regulates the epithelial-mesenchymal transition in lung cancer. *Oncogene* 30:3682–3693
2. Shih JY, Yang PC (2011) The EMT regulator slug and lung carcinogenesis. *Carcinogenesis* 32:1299–1304
3. Alves CC, Carneiro F, Hoefler H, Becker KF (2009) Role of the epithelial-mesenchymal transition regulator Slug in primary human cancers. *Front Biosci* 14:3035–3050
4. Becker KF, Rosivatz E, Blechschmidt K, Kremmer E, Sarbia M, Hoffer H (2007) Analysis of the E-cadherin repressor Snail in primary human cancers. *Cells Tissues Organs* 185:204–212
5. Folkman J (1996) New perspectives in clinical oncology from angiogenesis research. *Eur J Cancer* 32A:2534–2539
6. Buckley DL, Drew PJ, Mussurakis S, Monson JR, Horsman A (1997) Microvessel density of invasive breast cancer assessed by dynamic Gd-DTPA enhanced MRI. *J Magn Reson Imaging* 7:461–464
7. Knopp MV, Weiss E, Sinn HP, Mattern J, Junkermann H, Radeleff J, Magener A, Brix G, Delorme S, Zuna I et al (1999) Pathophysiologic basis of contrast enhancement in breast tumors. *J Magn Reson Imaging* 10:260–266
8. Tuncbilek N, Tokatli F, Altaner S, Sezer A, Ture M, Omurlu IK, Temizoz O (2011) Prognostic value DCE-MRI parameters in predicting factor disease free survival and overall survival for breast cancer patients. *Eur J Radiol* 81(5):863–867
9. Tuncbilek N, Karakas HM, Altaner S (2004) Dynamic MRI in indirect estimation of microvessel density, histologic grade, and prognosis in colorectal adenocarcinomas. *Abdom Imaging* 29:166–172
10. Guo J, Reddick WE, Glass JO, Ji Q, Billups CA, Wu J, Hoffer FA, Kaste SC, Jenkins JJ, Ortega Flores XC et al (2011) Dynamic contrast-enhanced magnetic resonance imaging as a prognostic factor in predicting event-free and overall survival in pediatric patients with osteosarcoma. *Cancer* 118(15):3376–3385

11. Tofts PS, Kermode AG (1991) Measurement of the blood-brain barrier permeability and leakage space using dynamic MR imaging. 1. Fundamental concepts. *Magn Reson Med* 17:357–367
12. Tofts PS, Brix G, Buckley DL, Evelhoch JL, Henderson E, Knopp MV, Larsson HB, Lee TY, Mayr NA, Parker GJ et al (1999) Estimating kinetic parameters from dynamic contrast-enhanced T(1)-weighted MRI of a diffusable tracer: standardized quantities and symbols. *J Magn Reson Imaging* 10:223–232
13. Sturn A, Quackenbush J, Trajanoski Z (2002) Genesis: cluster analysis of microarray data. *Bioinformatics* 18:207–208
14. Zijlstra A, Mellor R, Panzarella G, Aimes RT, Hooper JD, Marchenko ND, Quigley JP (2002) A quantitative analysis of rate-limiting steps in the metastatic cascade using human-specific real-time polymerase chain reaction. *Cancer Res* 62:7083–7092
15. Hong TM, Chen YL, Wu YY, Yuan A, Chao YC, Chung YC, Wu MH, Yang SC, Pan SH, Shih JY et al (2007) Targeting neuropilin 1 as an antitumor strategy in lung cancer. *Clin Cancer Res* 13:4759–4768
16. Yuan A, Lin CY, Chou CH, Shih CM, Chen CY, Cheng HW, Chen YF, Chen JJ, Chen JH, Yang PC et al (2011) Functional and structural characteristics of tumor angiogenesis in lung cancers overexpressing different VEGF isoforms assessed by DCE- and SSCE-MRI. *PLoS ONE* 6:e16062
17. Massague J (2008) TGFbeta in Cancer. *Cell* 134:215–230
18. Hynes RO (2002) A reevaluation of integrins as regulators of angiogenesis. *Nat Med* 8:918–921
19. Eliceiri BP, Cheresh DA (2001) Adhesion events in angiogenesis. *Curr Opin Cell Biol* 13:563–568
20. Stetler-Stevenson WG (1999) Matrix metalloproteinases in angiogenesis: a moving target for therapeutic intervention. *J Clin Invest* 103:1237–1241
21. Lee S, Jilani SM, Nikolova GV, Carpizo D, Iruela-Arispe ML (2005) Processing of VEGF-A by matrix metalloproteinases regulates bioavailability and vascular patterning in tumors. *J Cell Biol* 169:681–691
22. Ferrara N (2002) VEGF and the quest for tumour angiogenesis factors. *Nat Rev Cancer* 2:795–803
23. Bussolino F, Albini A, Camussi G, Presta M, Viglietto G, Ziche M, Persico G (1996) Role of soluble mediators in angiogenesis. *Eur J Cancer* 32A:2401–2412
24. Shao W, Wang W, Xiong XG, Cao C, Yan TD, Chen G, Chen H, Yin W, Liu J, Gu Y et al (2011) Prognostic impact of MMP-2 and MMP-9 expression in pathologic stage IA non-small cell lung cancer. *J Surg Oncol* 104:841–846
25. Shin SY, Kim JH, Baker A, Lim Y, Lee YH (2010) Transcription factor Egr-1 is essential for maximal matrix metalloproteinase-9 transcription by tumor necrosis factor alpha. *Mol Cancer Res* 8:507–519
26. Hegele A, Heidenreich A, Kropf J, von Knobloch R, Varga Z, Hofmann R, Olbert P (2004) Plasma levels of cellular fibronectin in patients with localized and metastatic renal cell carcinoma. *Tumour Biol* 25:111–116
27. Han JY, Kim HS, Lee SH, Park WS, Lee JY, Yoo NJ (2003) Immunohistochemical expression of integrins and extracellular matrix proteins in non-small cell lung cancer: correlation with lymph node metastasis. *Lung Cancer* 41:65–70
28. Jakowlew SB, Mariano JM, You L, Mathias A (1997) Differential regulation of protease and extracellular matrix protein expression by transforming growth factor-beta 1 in non-small cell lung cancer cells and normal human bronchial epithelial cells. *Biochim Biophys Acta* 1353:157–170
29. Han S, Khuri FR, Roman J (2006) Fibronectin stimulates non-small cell lung carcinoma cell growth through activation of Akt/mammalian target of rapamycin/S6 kinase and inactivation of LKB1/AMP-activated protein kinase signal pathways. *Cancer Res* 66:315–323
30. Kim S, Bell K, Mousa SA, Varner JA (2000) Regulation of angiogenesis in vivo by ligation of integrin alpha5beta1 with the central cell-binding domain of fibronectin. *Am J Pathol* 156:1345–1362
31. Yang Z, Zhang X, Gang H, Li X, Li Z, Wang T, Han J, Luo T, Wen F, Wu X (2007) Up-regulation of gastric cancer cell invasion by twist is accompanied by N-cadherin and fibronectin expression. *Biochem Biophys Res Commun* 358:925–930
32. Jia D, Yan M, Wang X, Hao X, Liang L, Liu L, Kong H, He X, Li J, Yao M (2010) Development of a highly metastatic model that reveals a crucial role of fibronectin in lung cancer cell migration and invasion. *BMC Cancer* 10:364
33. De Larco JE, Wuertz BR, Furcht LT (2004) The potential role of neutrophils in promoting the metastatic phenotype of tumors releasing interleukin-8. *Clin Cancer Res* 10:4895–4900
34. Petreaca ML, Yao M, Liu Y, Defea K, Martins-Green M (2007) Transactivation of vascular endothelial growth factor receptor-2 by interleukin-8 (IL-8/CXCL8) is required for IL-8/CXCL8-induced endothelial permeability. *Mol Biol Cell* 18:5014–5023
35. Huang S, Mills L, Mian B, Tellez C, McCarty M, Yang XD, Gudas JM, Bar-Eli M (2002) Fully humanized neutralizing antibodies to interleukin-8 (ABX-IL8) inhibit angiogenesis, tumor growth, and metastasis of human melanoma. *Am J Pathol* 161:125–134
36. Shi Q, Abbruzzese JL, Huang S, Fidler IJ, Xiong Q, Xie K (1999) Constitutive and inducible interleukin 8 expression by hypoxia and acidosis renders human pancreatic cancer cells more tumorigenic and metastatic. *Clin Cancer Res* 5:3711–3721
37. Inoue K, Slaton JW, Kim SJ, Perrotte P, Eve BY, Bar-Eli M, Radinsky R, Dinney CP (2000) Interleukin 8 expression regulates tumorigenicity and metastasis in human bladder cancer. *Cancer Res* 60:2290–2299
38. Mian BM, Dinney CP, Bermejo CE, Sweeney P, Tellez C, Yang XD, Gudas JM, McConkey DJ, Bar-Eli M (2003) Fully human anti-interleukin 8 antibody inhibits tumor growth in orthotopic bladder cancer xenografts via down-regulation of matrix metalloproteinases and nuclear factor-kappaB. *Clin Cancer Res* 9:3167–3175
39. Strieter RM, Belperio JA, Phillips RJ, Keane MP (2004) CXC chemokines in angiogenesis of cancer. *Semin Cancer Biol* 14:195–200
40. Belperio JA, Keane MP, Arenberg DA, Addison CL, Ehlert JE, Burdick MD, Strieter RM (2000) CXC chemokines in angiogenesis. *J Leukoc Biol* 68:1–8
41. Six I, Kureishi Y, Luo Z, Walsh K (2002) Akt signaling mediates VEGF/VPF vascular permeability in vivo. *FEBS Lett* 532:67–69
42. Galaup A, Cazes A, Le Jan S, Philippe J, Connault E, Le Coz E, Mekid H, Mir LM, Opolon P, Corvol P et al (2006) Angiotensin-like 4 prevents metastasis through inhibition of vascular permeability and tumor cell motility and invasiveness. *Proc Natl Acad Sci USA* 103:18721–18726
43. Westhoff B, Colaluca IN, D'Ario G, Donzelli M, Tosoni D, Volorio S, Pelosi G, Spaggiari L, Mazzarol G, Viale G et al (2009) Alterations of the Notch pathway in lung cancer. *Proc Natl Acad Sci USA* 106:22293–22298
44. Sahlgren C, Gustafsson MV, Jin S, Poellinger L, Lendahl U (2008) Notch signaling mediates hypoxia-induced tumor cell migration and invasion. *Proc Natl Acad Sci USA* 105:6392–6397
45. Erler JT, Bennewith KL, Nicolau M, Dornhofer N, Kong C, Le QT, Chi JT, Jeffrey SS, Giaccia AJ (2006) Lysyl oxidase is essential for hypoxia-induced metastasis. *Nature* 440:1222–1226
46. Gao Y, Xiao Q, Ma H, Li L, Liu J, Feng Y, Fang Z, Wu J, Han X, Zhang J et al (2010) LKB1 inhibits lung cancer progression through lysyl oxidase and extracellular matrix remodeling. *Proc Natl Acad Sci USA* 107:18892–18897

47. Wilgus ML, Borczuk AC, Stoopler M, Ginsburg M, Gorenstein L, Sonett JR, Powell CA (2011) Lysyl oxidase: a lung adenocarcinoma biomarker of invasion and survival. *Cancer* 117:2186–2191
48. Shankar J, Messenberg A, Chan J, Underhill TM, Foster LJ, Nabi IR (2010) Pseudopodial actin dynamics control epithelial-mesenchymal transition in metastatic cancer cells. *Cancer Res* 70:3780–3790
49. Nakao A, Afrakhte M, Moren A, Nakayama T, Christian JL, Heuchel R, Itoh S, Kawabata M, Heldin NE, Heldin CH et al (1997) Identification of Smad7, a TGFbeta-inducible antagonist of TGF-beta signalling. *Nature* 389:631–635
50. Hayashi H, Abdollah S, Qiu Y, Cai J, Xu YY, Grinnell BW, Richardson MA, Topper JN, Gimbrone MA Jr, Wrana JL et al (1997) The MAD-related protein Smad7 associates with the TGFbeta receptor and functions as an antagonist of TGFbeta signaling. *Cell* 89:1165–1173
51. Kavsak P, Rasmussen RK, Causing CG, Bonni S, Zhu H, Thomsen GH, Wrana JL (2000) Smad7 binds to Smurf2 to form an E3 ubiquitin ligase that targets the TGF beta receptor for degradation. *Mol Cell* 6:1365–1375